

Mechanical properties of Ti–W alloys reinforced with TiC particles

Heeman Choe^{a,*}, Susan Abkowitz^b, Stanley M. Abkowitz^b, David C. Dunand^c

^a School of Advanced Materials Engineering, Kookmin University, Chungneung-dong, Songbuk-ku, Seoul 136-702, South Korea

^b Dynamet Technology Inc., Eight A Street, Burlington, MA 01803, USA

^c Department of Materials Science and Engineering, Northwestern University, Evanston, IL 60208, USA

Received 23 August 2007; received in revised form 14 January 2008; accepted 24 January 2008

Abstract

Composites consisting of a Ti–W solid-solution-strengthened matrix reinforced with TiC particles are produced by powder metallurgy. TiC additions increase strength but reduce ductility and matrix microhardness. Composites with 7.5 wt.% TiC show some tensile ductility (3–7%) but those with 15 wt.% TiC are brittle in tension. They are however strong and ductile in compression: Ti–15W/15TiC (wt.%) has a compressive yield strength exceeding 1200 MPa. This composite also shows tensile crack growth rates which are considerably faster than for pure titanium (by a factor 2) or Ti–15W (by a factor 2–6) and a fracture toughness which remains relatively high as compared to Ti–15W (21 vs. 34 MPa $\sqrt{\text{m}}$).

© 2008 Elsevier B.V. All rights reserved.

Keywords: Titanium alloy; Composite; Orthopedic; Powder metallurgy; Mechanical properties; Titanium carbide

1. Introduction

Titanium and its alloys are used extensively for biomedical implants due to their excellent mechanical properties, corrosion resistance and biocompatibility [1–4]. Moreover, their stiffness (~80–130 GPa [5]) is substantially lower than that of other conventional metallic implant materials such as stainless steel (~190–200 GPa [5]) or Co alloys (~200–248 GPa [5]), thus reducing the stress shielding effect arising from differences in compliance between bone (~10–40 GPa [6]) and implant [7,8]. While used for some low-stress bone implants [9,10], commercially pure titanium (CP-Ti) suffers from a relatively low strength and poor wear resistance, making it inadequate for highly stressed bone implants or wear-prone prostheses [11]. Hardness and wear resistance, and to a lesser extent strength, can be improved by the addition of TiC particles to CP-Ti [12–20]; however, these Ti–TiC composites, in line with other metal matrix composites [21], show reduced ductility and fracture toughness [12–14,22].

Recently, the use of tungsten as a solid-solution strengthener in CP-Ti has been found to result in large increases in strength and hardness with only moderate decrease in ductility [23,24]. For the two alloys studied to date, Ti–10 wt.% W exhibits

a stress–strain curve similar to Ti–6Al–4V (yield strength $\sigma_y = 770$ –800 MPa and ductility $\epsilon_f = 14.1$ –18.5% [23,24]) while Ti–15 wt.% W is stronger but less ductile ($\sigma_y = \sim 1000$ MPa and $\epsilon_f = \sim 9\%$). While Ti–W alloys are also harder than CP-Ti, they are not expected to achieve the high levels of hardness and wear resistance needed for some of the above implant applications [25].

Here, we investigate the effect of adding TiC particles to Ti–W alloys, with the goal of striking a balance between the gain in hardness and wear resistance and the penalty in ductility and toughness provided by the ceramic reinforcement. We report on the microstructure and room-temperature mechanical properties of five composites consisting of Ti matrices alloyed with 0, 7.5 or 15 wt.% W and containing 7.5 or 15 wt.% TiC particles.

2. Experimental procedures

2.1. Processing and microstructure

As summarized in Table 1, five TiC-containing composites with Ti–7.5W or Ti–15W matrix and two TiC-free control alloys CP-Ti and Ti–15W (all compositions are given in wt.% in the following) were created by the combined cold and hot isostatic pressing (CHIP) process [26]. Ti powders (<150 μm), W powders and TiC powders (both <10 μm) were blended and compacted into billets by cold isostatic pressing at a pressure of

* Corresponding author. Tel.: +82 2 910 4417; fax: +82 2 910 4320.
E-mail address: heeman@kookmin.ac.kr (H. Choe).

Table 1
Tensile properties (compressive yield stresses given in parentheses), fracture toughness and matrix microhardness

Alloy	W (wt.%)	TiC (wt.%)	0.2% yield stress (MPa)	Ultimate tensile stress (MPa)	Tensile strain at failure (%)	Matrix hardness (HV)	Fracture toughness (MPa \sqrt{m})
CP-Ti	0	0	411 ^a	518 ^a	24 ^a	210 \pm 20 ^a	45.0 ^b
Ti-15W	15	0	1085	1168	8.8	461 \pm 26	34.2
Ti/7.5TiC	0	7.5	689	714	6.9	375 \pm 41	
Ti-7.5W/7.5TiC	7.5	7.5	709	759	2.9	349 \pm 35	
Ti-15TiC	0	15	648 (663 ^c)	698	1.2 ^d	283 \pm 48	
Ti-7.5W/15TiC	7.5	15	>671 (746 ^c)	692	0.7 ^d	278 \pm 15	
Ti-15W/15TiC	15	15	>739 (1214 ^c)	739	0.6 ^d	297 \pm 7	20.8

^a See Ref. [23].

^b K_Q .

^c Compression.

^d Premature failure.

379 MPa. The billets were vacuum-sintered at 1230 °C for 4 h and densified by hot isostatic pressing (HIP) at 900 °C for 2 h at 100 MPa [27], followed by slow cooling within the press. They were then annealed in vacuum at 732 °C for 1 h and furnace-cooled.

The billet microstructures were evaluated by optical microscopy on polished cross-sections etched with a modified Kroll's reagent (5% nitric acid, 10% HF, and 85% water). Chemical composition profiles were measured by energy-dispersive spectroscopy (EDS, Hitachi S-3500) with a spot size of 15 nm and a voltage in the range of 15–20 kV.

2.2. Mechanical testing

Matrix microhardness was determined with a Vickers indenter using a 200 g load and an indent time of 10 s on epoxy-mounted cross-sections of the material polished to 0.05 μm with colloidal alumina. Hardness measurements were taken in the matrix far from any residual tungsten and titanium carbide particles. Tensile tests were performed on one specimen of each composition (except CP-Ti for which prior data [23] were used), machined to ASTM E-8 proportional standards [28] with 36 mm gauge length and 6.4 mm gauge diameter. The cross-head speed was 12.7 mm/min, corresponding to an initial strain rate of $6.2 \times 10^{-3} \text{ s}^{-1}$. The strain was measured with an extensometer with 25.4 mm gauge length. Additionally, the three composites with 15 wt.% TiC, which had displayed premature tensile failure, were tested in compression on cylinders with a diameter of 7 mm and an aspect ratio of 3:1 according to ASTM standards E-9 [29]. The tests were carried out to strains of over 13%, maintaining a low strain rate of $1 \times 10^{-4} \text{ s}^{-1}$.

CP-Ti, Ti-15W and Ti-15W/15TiC were machined for three-point bend test to dimensions 7 mm \times 14 mm \times 50 mm. They were polished down to 0.05 μm finish, and subjected to fracture toughness testing in general accordance with the ASTM standard E-399 [30] for plane-strain fracture toughness. Prior to the bend test, a fatigue pre-crack was grown out of the machined notch in each sample by cycling at a load ratio of 0.1 ($R = K_{\min}/K_{\max}$, where K_{\max} and K_{\min} are, respectively, the maximum and minimum stress intensities in the fatigue cycle) and

loading frequency of 1 Hz. Actual fatigue data were collected after well over 1 mm growth of pre-crack to eliminate the effect of the machined starter notch [31]. A load-drop technique was manually used to attempt to reach the fatigue threshold as recommended by ASTM E-647 [31]: the load was dropped by less than 5% every 300 μm of crack propagation in order to minimize any crack retardation effect. A traveling microscope was used to measure the crack length manually during fatigue crack growth. The final crack length prior to the plane-strain fracture toughness test, defined as a notch crack plus a fatigue pre-crack, was 7 mm, approximately half of the specimen width (14 mm) according to ASTM standard E-399 [30]. An average value was taken between two opposite sides of a sample for toughness calculation. Samples were loaded to failure under displacement-control at a cross-head displacement rate of 0.6 mm/min. The applied loads and the corresponding displacements were recorded during the test and analyzed for the determination of plane-strain fracture toughness. Resulting fracture surfaces were also examined in a scanning electron microscope (SEM).

3. Results

3.1. Microstructure

Fig. 1(a–g) shows micrographs of etched cross-sections for the five composites and the two control alloys (CP-Ti and Ti-15W). The TiC particles are roughly equiaxed and reasonably uniformly distributed for the composites with 7.5 wt.% TiC. Clustering is more pronounced in the composites with 15 wt.% TiC. Upon alloying with W, the matrix shows an acicular structure after etching (Fig. 1b, d, f and g), which was previously reported as Widmanstätten α/β structure with most of the W segregated in the β -phase [23,24,32]. As previously reported in Refs. [23,24], W dissolution in the present alloys is anticipated to be complete, given the small W average powder sizes ($<10 \mu\text{m}$). In rare cases, partially dissolved W particles were observed, as shown in Fig. 1(b, d, f and g), which are surrounded by a dark-etched matrix shell corresponding to a diffusion zone with high W content. The shell hardness is lower than that of the matrix at a large distance from the particle (Fig. 2), with a

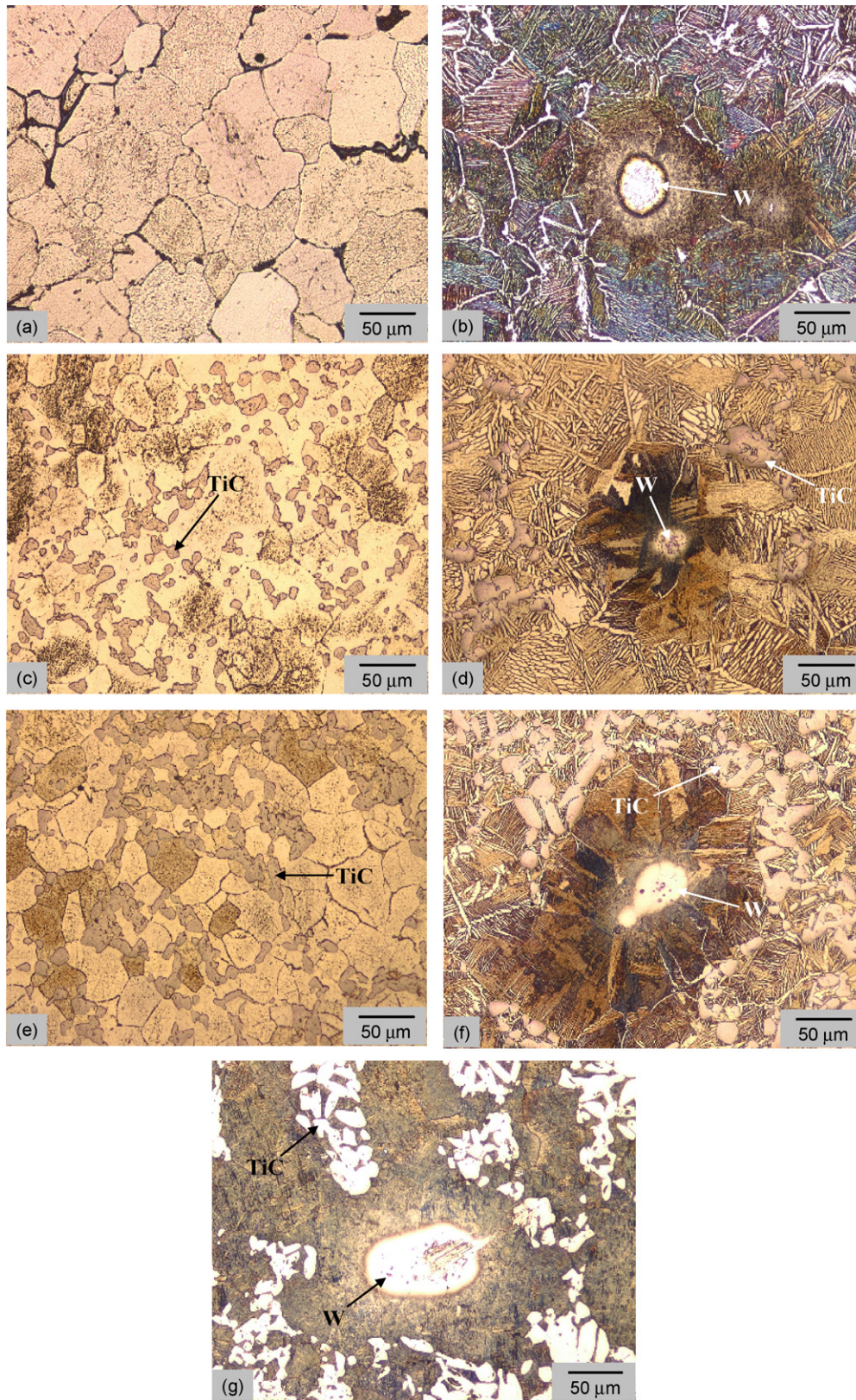


Fig. 1. Optical micrographs of etched microstructures: (a) CP-Ti, (b) Ti-15W, (c) Ti/7.5TiC, (d) Ti-7.5W/7.5TiC, (e) Ti/15TiC, (f) Ti-7.5W/15TiC and (g) Ti-15W/15TiC. TiC particles are marked with arrows. Micrographs of composites were selected to show W particles (marked with “W”) which were very rare in the cross-sections.

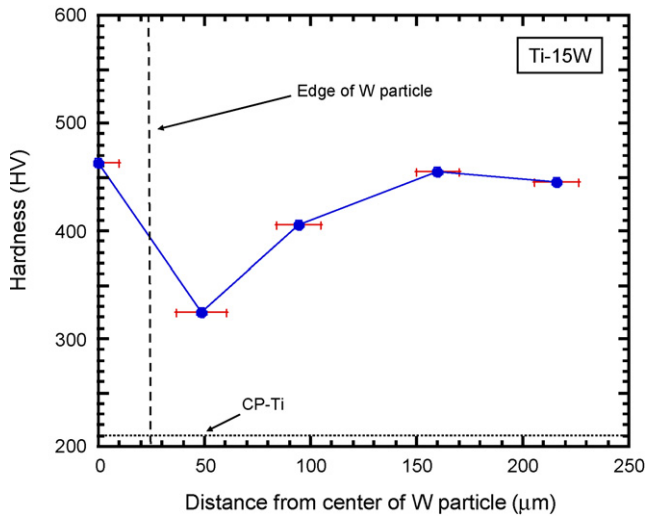


Fig. 2. Microhardness profile from the center of a W particle into the Ti matrix for Ti-15W.

value in agreement with average matrix values given in Table 1. The shape of the hardness profile of Fig. 2 for Ti-15W is similar to that of a profile measured previously on a Ti-10W alloy [24].

As shown in Fig. 3, the addition of TiC particles reduced the Ti-W matrix microhardness. The macrohardness of the composites was not measured but was expected to be significantly enhanced by the very hard TiC particles.

3.2. Tensile and compressive properties

Fig. 4(a) displays the engineering tensile stress–strain curves for all specimens and for a previously published CP-Ti sample produced by the same process [23]. The corresponding tensile properties are listed in Table 1. As expected, all five composites exhibit tensile yield and ultimate strengths higher than CP-Ti,

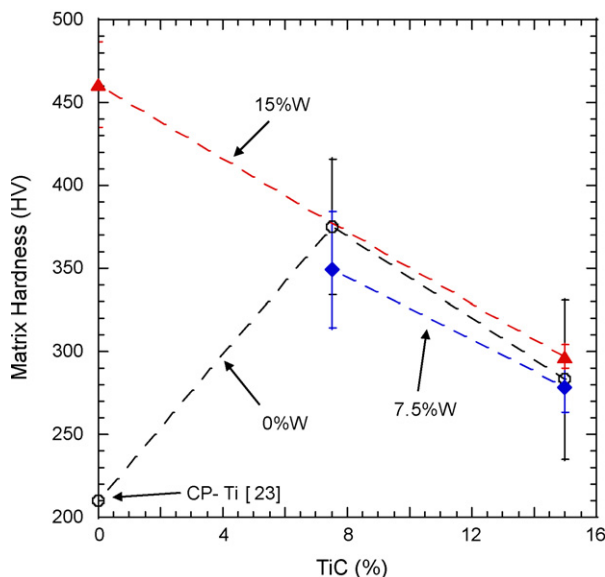


Fig. 3. Average matrix hardness values as a function of W and TiC contents for all samples in the present investigation and CP-Ti [23].

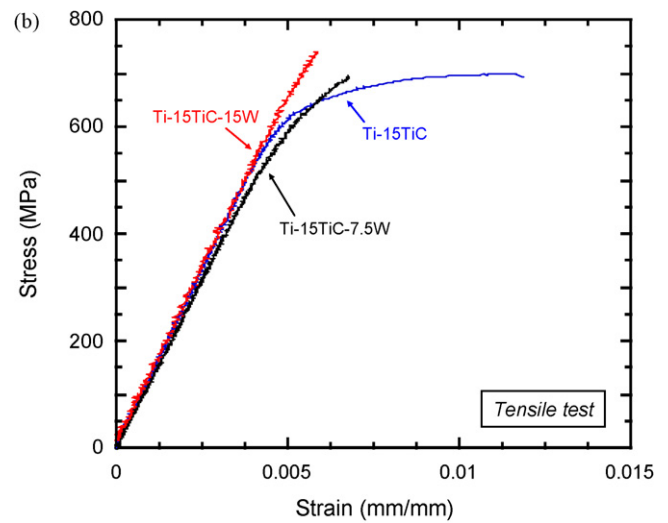
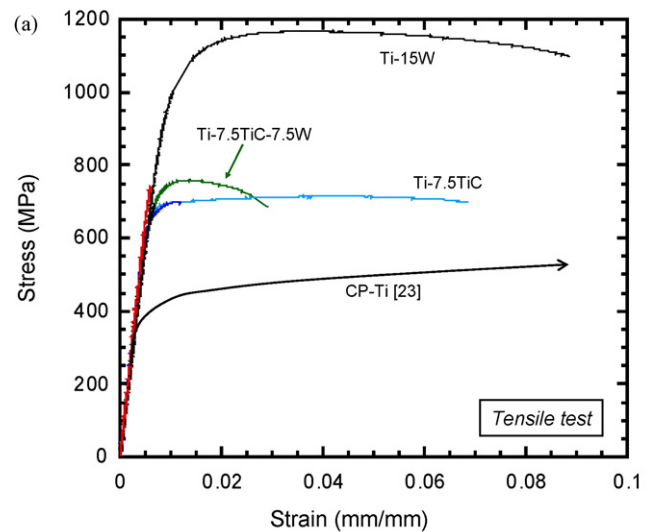


Fig. 4. Tensile stress-strain curves for (a) all samples and CP-Ti [23] and (b) composites with 15 wt.% TiC which exhibited premature failure.

but at the expense of decreased ductility. The two composites with 7.5% TiC have tensile yield and ultimate strengths comparable to or better than the three composites with 15% TiC, as a result of the premature failure of the specimens with 15% TiC content occurring before the yield point (for Ti-7.5W/15TiC and Ti-15W/15TiC) or shortly thereafter (for Ti/15TiC). The stress–strain curves for the composites with 15% TiC are shown in greater detail in Fig. 4(b). When tested in compression, however, their fracture is inhibited and higher yield strengths are achieved (Fig. 5), although a direct comparison may not be made between their tensile and compressive results due to a tension–compression asymmetry existing in Ti and its alloys [33].

3.3. Fracture toughness

Linear elastic stress intensity, K , was computed from the ASTM standard E-399 [30] for plane-strain fracture toughness

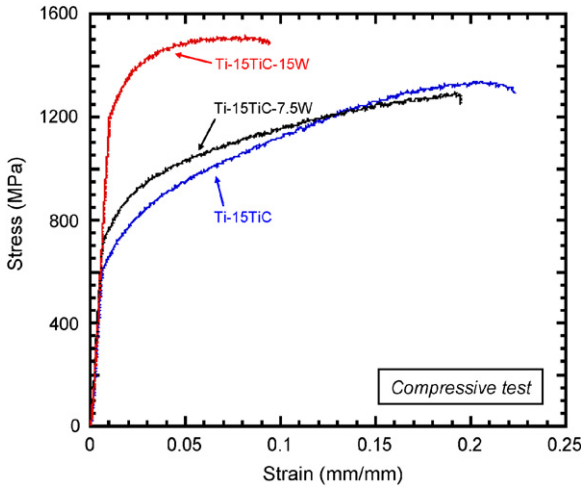


Fig. 5. Compressive stress–strain curves for composites with 15 wt.% TiC.

for the three-point bend specimen:

$$K = \left(\frac{PS}{BW^{3/2}} \right) f \left(\frac{a}{W} \right) \quad (1)$$

where P is the applied load, S is the distance between the outer loading pins, a is the crack length, B is the specimen thickness, W is the specimen width and $f(a/W)$ is a dimensionless factor [34]. The specimen was monotonically loaded under displacement-control to produce catastrophic failure in accordance with ASTM E-399 [30], once the fatigue crack had reached a significant length (approximately half of the specimen width). Results of the fracture toughness testing, in the form of typical test records of the load-versus-displacement curves, are shown in Fig. 6 for CP-Ti, Ti–15W and Ti–15W/15TiC. In particular, the crack length for CP-Ti increased significantly until the point of maximum load: the crack growth was maintained stably by the displacement-controlled nature of the test. Using

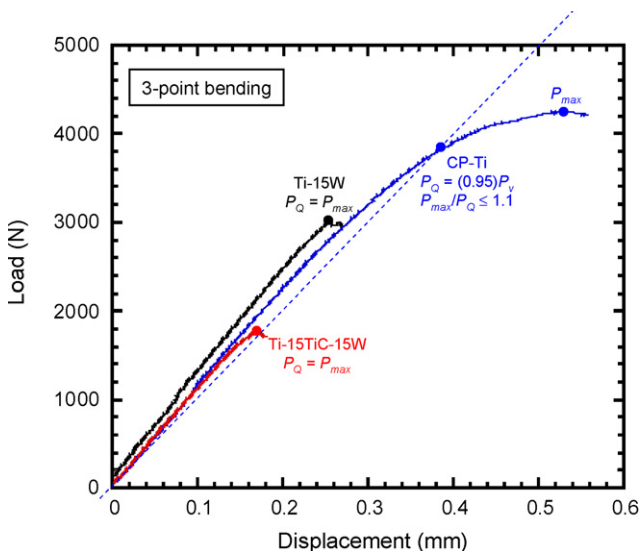


Fig. 6. Load–displacement curves obtained for the measurement of the fracture toughness after a fatigue pre-crack for CP-Ti, Ti–15W and Ti–15W/15TiC.

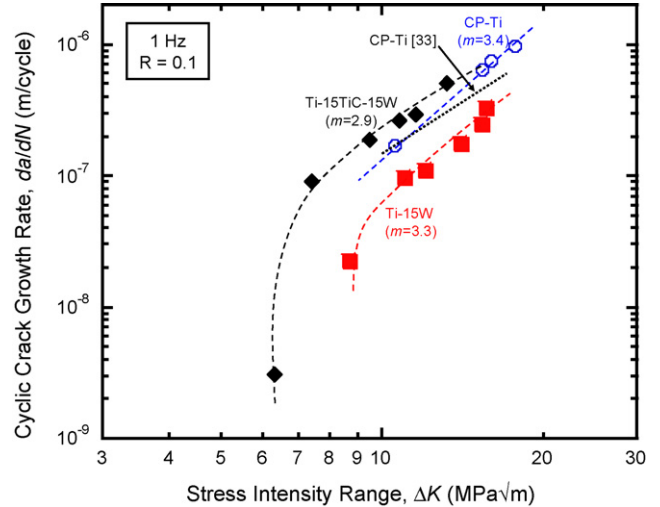


Fig. 7. Variation in cyclic fatigue-crack propagation rates, da/dN , as a function of the applied stress intensity range, ΔK for CP-Ti, Ti–15W and Ti–15W/15TiC. Shown for comparison are literature data for CP-Ti [33].

Eq. (1), the ‘conditional’ fracture toughness was calculated from the measured critical loads, P_Q , for the onset of unstable fracture as $K_Q = 45, 34$ and $21 \text{ MPa}\sqrt{\text{m}}$ for CP-Ti, Ti–15W and Ti–15W/15TiC, respectively.

3.4. Fatigue crack propagation

As recommended in Ref. [31], constant force amplitude procedure for $da/dN > 10^{-8} \text{ m/cycle}$ was adopted for collecting crack growth data. Additionally, attempts were made to acquire fatigue threshold values (ΔK_{th}) using load-dropping technique manually [31]. Once the assumed threshold was reached, the load was kept constant to gradually increase the stress intensity. The crack growth behavior during the load-ascending test was similar to that exhibited during the load-shedding, indicating no or little crack retardation by the crack tip plasticity after each load-drop [31]. The variation in fatigue-crack propagation rates (average crack extension per cycle) with the applied stress intensity range for CP-Ti, Ti–15W and Ti–15W/15TiC is shown in Fig. 7. It is apparent that the fatigue crack growth properties of Ti–15W are superior to those of both CP-Ti and Ti–15W/15TiC. The true value of fatigue crack growth threshold, ΔK_{th} (i.e., ΔK at fatigue crack growth rate less than 10^{-10} m/cycle), could not be obtained due to the lack of sample availability and the difficulties associated with manual testing operation. Crack growth rates in these alloys exhibited comparatively low sensitivity to the stress intensity, as is typically observed in most metallic materials. Using the Paris power–law relationship:

$$\frac{da}{dN} = C \Delta K^m \quad (2)$$

where C and m are scaling constants, the Paris exponents for CP-Ti, Ti–15W, and Ti–15W/15TiC are, respectively, $m = 3.4, 3.3$, and 2.9 , all of which fall in the range of typical metallic materials with $m = 2–4$ [36].

4. Discussion

4.1. Effect of microstructure on hardness and tensile/compressive properties

Due to the complete solubility between Ti and W above 882 °C and the fine W powder size, the sintering and HIP steps at 1230 °C are expected to achieve near-complete dissolution of the W powders into the Ti matrix, giving rise to the Widmanstätten α/β structure visible in Fig. 1 and the marked strengthening effect observed in Ti–15W in Fig. 4, as reported previously [23,24]. On rare occasions, partially dissolved W particles surrounded by a matrix diffusion zone were also observed, as shown in Fig. 1(b, d, f and g). These most probably belong to a small population of W particles much larger than average (as expected in commercially sieved powders), which were not fully dissolved during the sintering and HIP steps.

It is apparent from Table 1 that the tensile yield strengths of composites with low TiC content (Ti/7.5TiC and Ti–7.5W/7.5TiC) are comparable to the respective compressive yield strengths of the high TiC composites (Ti/15TiC and Ti–7.5W/15TiC). The lack of composite strengthening upon doubling TiC content from 7.5 to 15 wt.% may be due in part to the clustering of TiC particles shown in Fig. 1(g), which is also partially responsible for the drop in ductility observed for the high TiC composites.

Fig. 3 indicates that, with increasing TiC content, the hardness of the matrix of the W-containing composite decreases substantially. For the two composites without W, the hardness values are almost within error: 375 ± 41 for Ti/7.5TiC and 283 ± 48 for Ti/15TiC. However, for the composites with W, the drop seems to be significant. It may be explained by the fact that TiC dissolved into titanium at 1230 °C until the maximum solid solubility of carbon was reached (which is ~ 1 at.% in pure Ti [37]) but is not known in Ti–W alloys). This dissolved carbon may have affected the precipitation sequence on cooling, leading to a change in the Widmanstätten α/β structure [38] and a drop in matrix hardness (unlike the effect of C dissolution in CP-Ti, which increases hardness, Fig. 3). This drop in Ti–W matrix hardness may also explain the decrease in tensile yield strength observed upon doubling TiC content from Ti–7.5W/7.5TiC ($\sigma_y = 709$ MPa) to Ti–7.5W/15TiC ($\sigma_y = 671$ MPa): the composite strengthening resulting from increasing TiC content is negated by the softening of the matrix.

At constant TiC content, the compressive yield stress of the composites increases with W content, from 663 MPa for Ti/15TiC to 746 MPa for Ti–7.5W/15TiC to 1214 MPa for Ti–15W/15TiC, indicating that W solid solution strengthening can improve the compressive strength even in the presence of high amounts of TiC. However, only TiC particles can provide the higher macro hardness and wear resistance needed for some biomedical implant applications.

Some TiC clustering is observed in all composites in this study (Fig. 1(c–g)) but is more pronounced in composites with the higher level, 15% TiC. Such TiC clustering was also reported in Ti–6Al–4V reinforced with 10% TiC [38]. Indeed, it has been noted that it is difficult to achieve a homogeneous distribution

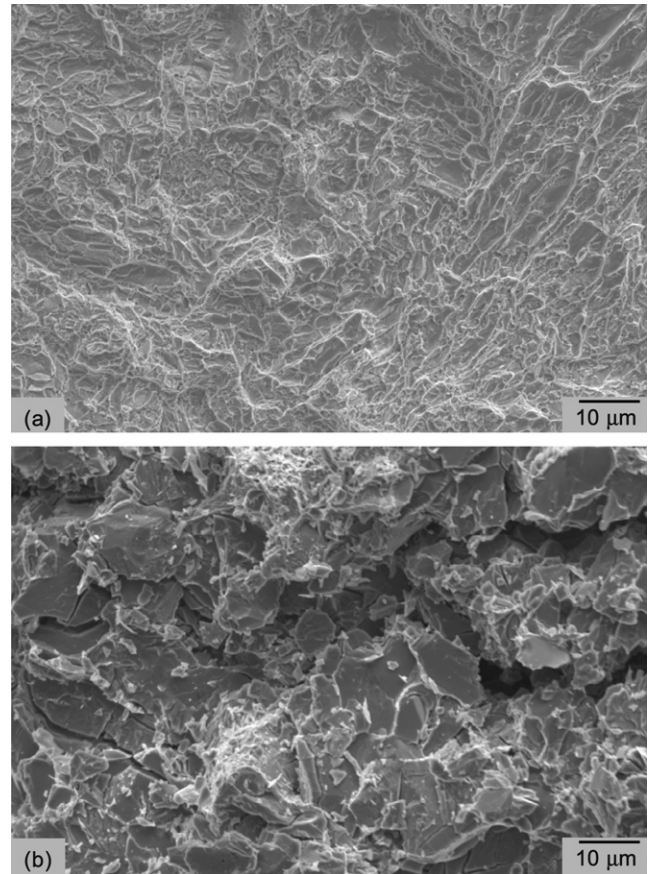


Fig. 8. SEM micrographs of tensile fracture surfaces showing (a) ductile failure in Ti–15W and (b) brittle fracture associated with a number of microcracks in Ti–15W/15TiC.

of ceramic particles in composite materials using conventional powder metallurgy methods [39]. It has also been confirmed by a number of authors [40–44] that particle clustering can greatly reduce the ductility and flow stress of composites due to reinforcement fracture followed by the onset of plastic instability at low strains. As expected, the tensile fracture surface of Ti–15W/15TiC is brittle, as evidenced by the presence of fractured clustered TiC particles and numerous secondary cracks (Fig. 8b). By contrast, the fracture surface for Ti–15W has a ductile appearance, and is characterized by coalescence of microvoids and dimples (Fig. 8a).

4.2. Fracture toughness

According to ASTM E-399 [30], plasticity at the crack tip must be small compared to specimen geometry and crack length in order to ensure the validity of plane-strain fracture toughness condition. In other words, for the calculated K_Q values to be equal to K_{Ic} , both the specimen thickness, B , and the crack length, a , must be larger than $2.5(K_c/\sigma_y)^2$, where K_c is the fracture toughness of the material, i.e., much larger than the plastic or damage zone size $r_y \approx (1/2)\pi(K_c/\sigma_y)^2$. Both Ti–15W and Ti–15W/15TiC samples pass the plane-strain condition requirement with $2.5(K_c/\sigma_y)^2 = 2.5$ and 1.98 mm, respectively, using tensile yield strength in both cases. Their

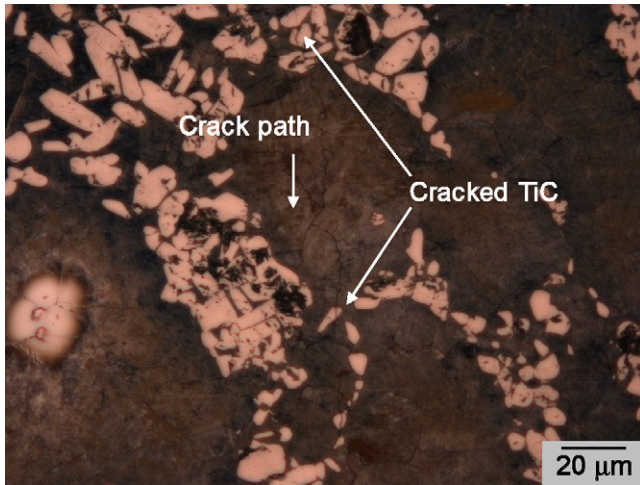


Fig. 9. Optical micrograph of the cyclic fatigue region of three-point bend samples of Ti–15W/15TiC. The nominal direction of crack growth is also indicated.

fracture toughness is thus $K_{Ic} = 34$ and $21 \text{ MPa } \sqrt{\text{m}}$, respectively. CP-Ti does not meet the criterion (with $2.5(K_c/\sigma_y)^2 = 9.1 \text{ mm}$ somewhat larger than $a = 7.1 \text{ mm}$ and $B = 7.0 \text{ mm}$). However, because this criterion is generally considered quite conservative and the calculated damage zone ($r_y = 1.9 \text{ mm}$) is well below the specimen dimensions, it is believed that the toughness value obtained with the current tested sample for CP-Ti ($K_Q = 45 \text{ MPa } \sqrt{\text{m}}$) is close to a lower bound of the fracture toughness [45].

The crack path in TiC-reinforced composites is reported to be strongly influenced by the fracture of TiC particles [38,46]. Therefore, the drop in fracture toughness of Ti–15W/15TiC as compared to CP-Ti and Ti–15W is likely due to the presence of brittle TiC phase: their resistance against crack propagation is significantly lower than the matrix as was also observed in fracture surfaces in Fig. 8. Fig. 9 shows the crack propagation path through TiC particles in Ti–15W/15TiC, which confirms that TiC particles in Ti–15W/15TiC were fractured during crack advance. Moreover, since particles are unevenly distributed in the Ti matrix of Ti–15W/15TiC, as described earlier and shown in Fig. 1(g), this may have provided a preferential path for the crack propagation [38]. Whether or not the crack indeed favored any preferential path through TiC particles or the occasional W-rich region was not examined quantitatively in this investigation.

4.3. Fatigue crack propagation

In the Paris law regime (i.e., typically between 10^{-9} and 10^{-6} m/cycle) Ti–15W exhibits greater cyclic fatigue resistance than CP-Ti (Fig. 7). This can be attributed to the intrinsic toughening mechanism active in the alloy, i.e., solid solution strengthening provided by W, as is apparent by the higher strength of Ti–15W. It may also be linked to the superior resistance to fatigue crack propagation of the Widmanstätten α/β microstructure present in Ti–15W (Fig. 1(b)) over the equiaxed α structure visible in CP-Ti (Fig. 1(a)) [47].

In the Paris regime, the Ti–15W/15TiC composites displayed somewhat faster crack growth rate (by a factor of 2–6) than

Ti–15W, and almost the same growth rate than CP-Ti, whose fatigue behavior is in good agreement with literature data [35], as shown in Fig. 7. The faster crack growth rate in Ti–15W/15TiC compared to Ti–15W and CP-Ti at high ΔK can be explained by the fact that the composite reaches crack growth instability at lower K_{max} values due to its lower fracture toughness [48]. For low ΔK , the fatigue threshold value for the composite seems to be near $6 \text{ MPa } \sqrt{\text{m}}$, while the lowest data point for the Ti–15W may correspond to the start of the inflection leading to a threshold value near $8 \text{ MPa } \sqrt{\text{m}}$, as illustrated with a vertical dotted line in Fig. 7. At low crack growth rates, particularly near fatigue threshold, there are some cases where composites are reported to exhibit superior fatigue performance than their monolithic matrix, as reinforcement particles provide crack deflection, meandering, or roughness-induced closure [48,49]. However, particulate reinforcements have sometimes been found to worsen fatigue propagation behavior in composites [50,51], due to factors such as change in microstructure, composition and processing. In the present case, the inferior fatigue properties of Ti–15W/15TiC at lower crack growth rates may be due to the brittle nature of the TiC particles and their inability to provide crack growth resistance through roughness-induced closure, as observed in Fig. 9.

5. Conclusions

Following earlier work by the authors investigating either TiC or W additions to CP-Ti by powder metallurgy, TiC particles (7.5 or 15 wt.%) were added to Ti–W (7.5 and 15 wt.%) solid-solution-strengthened alloys, to enhance macrohardness and wear resistance. As expected, TiC additions result in increased yield strength but reduced ductility: composites with 7.5% TiC show reduced, but still useful, tensile ductilities (3–7%), while those with 15% TiC are near brittle in tension, but exhibit ductile behavior in compression and very high compressive yield strength. It was also observed that the matrix microhardness drops with increasing TiC, probably as a result of carbon dissolution affecting its transformation behavior.

A Ti–15% W/15% TiC was further examined, due to its very high compressive yield strength of over 1200 MPa. As expected, the presence of TiC particles affects negatively the fatigue and fracture properties. The penalty in fatigue crack growth rate as compared to unreinforced Ti–15% W is relatively minor (a factor of 2–6), and may be due to reduced matrix hardness or fracture of the TiC particles ahead of the crack. While lower than the fracture toughness for the unreinforced Ti–15W ($34 \text{ MPa } \sqrt{\text{m}}$), the Ti–15W/15TiC composite exhibits a still useful value of $21 \text{ MPa } \sqrt{\text{m}}$.

Acknowledgement

This research was funded by the SBIR program of the US National Institute of Health through grant no. 2R44EB001005-02 to Dynamet Technology Inc. HC also acknowledges partial support from the 2007 research fund of Kookmin University in Korea.

References

- [1] H. Güleriyüz, H. Cimenoglu, *Biomaterials* 25 (2004) 3325.
- [2] M. Aziz-Kerrzo, K.G. Conroy, A.M. Fenelon, S.T. Farrell, C.B. Breslin, *Biomaterials* 22 (12) (2001) 1531.
- [3] Y. Okazaki, E. Gotoh, *Biomaterials* 26 (2005) 11.
- [4] A. Wisbey, P.J. Gregson, L.M. Peter, M. Tuke, *Biomaterials* 12 (1991) 470.
- [5] M.F. Ashby, D.R.H. Jones, *Engineering Materials 1: An Introduction to their Properties and Applications*, Pergamon Press, Oxford, 1987.
- [6] M.J. Long, H.J. Rack, *Biomaterials* 19 (1998) 1621.
- [7] J. Black, *Biological Performance of Materials: Fundamentals of Biocompatibility*, third ed., Marcel Dekker Inc., New York, 1999.
- [8] F.H. Silver, D.L. Christiansen, *Biomaterials Science and Biocompatibility*, Springer-Verlag, New York, 1999.
- [9] N.S. Peckitt, *Br. J. Oral. Maxillofac. Surg.* 37 (1999) 353.
- [10] J. Acero, J. Calderon, J.I. Salmeron, J.J. Verdager, C. Concejo, M.L. Somacarrera, *J. Craniomaxillofac. Surg.* 27 (1999) 117.
- [11] D. Iijima, T. Yoneyama, H. Doi, H. Hamanaka, N. Kurosaki, *Biomaterials* 24 (2003) 1519.
- [12] S. Abkowitz, S.M. Abkowitz, H. Fisher, P.J. Schwartz, *JOM* 56 (5) (2004) 37.
- [13] S. Abkowitz, P.F. Weihrauch, S.M. Abkowitz, H.L. Heussi, *JOM* 47 (8) (1995) 40.
- [14] S. Abkowitz, P. Weihrauch, *Adv. Mater. Process* 136 (1) (1989) 31.
- [15] Y. Liu, L.F. Chen, H.P. Tang, C.T. Liu, B. Liu, B.Y. Huang, *Mater. Sci. Eng. A* 418 (1–2) (2006) 25.
- [16] W.J. Lu, D. Zhang, X.N. Zhang, R.J. Wu, T. Sakata, H. Mori, *J. Alloy Compd.* 327 (1–2) (2001) 248.
- [17] D.C. Dunand, C.M. Bedell, *Acta Mater.* 44 (3) (1996) 1063.
- [18] M. Frary, C. Schuh, D.C. Dunand, *Metall. Mater. Trans. A* 33 (2002) 1669.
- [19] M. Hagiwara, N. Arimoto, S. Emura, Y. Kawabe, H.G. Suzuki, *Iron Steel Inst. Jpn.* 32 (1992) 909.
- [20] D.E. Alman, J.A. Hawk, *Wear* 225–229 (1999) 629.
- [21] D.J. Lloyd, *Int. Mater. Rev.* 39 (1) (1994) 1.
- [22] S. Ranganath, *J. Mater. Sci.* 32 (1) (1997) 1.
- [23] M. Frary, S. Abkowitz, S.M. Abkowitz, D.C. Dunand, *Mater. Sci. Eng. A* 344 (2003) 103.
- [24] H. Choe, S.M. Abkowitz, S. Abkowitz, D.C. Dunand, *J. Alloys Compd.* 390 (2005) 62.
- [25] R. Hübler, *Surf. Coat. Technol.* 116–119 (1999) 1111.
- [26] S. Abkowitz, P.F. Weihrauch, S.M. Abkowitz, *Ind. Heat* 12 (1993) 32.
- [27] W.F. Ho, C.P. Ju, J.H.C. Lin, *Biomaterials* 20 (1999) 2115.
- [28] Annual Book of ASTM Standards, vol. 03.01 (E-8), Standard Test Methods for Tension Testing of Metallic Materials, ASM International, Philadelphia, PA, 1994, p. 60.
- [29] Annual Book of ASTM Standards, vol. 03.01 (E-9), Standard Test Methods for Compression Testing of Metallic Materials, ASM International, Philadelphia, PA, 1994, p. 101.
- [30] Annual Book of ASTM Standards, vol. 03.01 (E-399), Standard Test Method for Plane-Strain Fracture Toughness of Metallic Materials, ASM International, Philadelphia, PA, 1997, p. 462.
- [31] Annual Book of ASTM Standards, vol. 03.01 (E-647), Standard Test Method for Measurement of Fatigue Crack Growth Rates, ASM International, Philadelphia, PA, 1997, p. 628.
- [32] H. Choe, S.M. Abkowitz, S. Abkowitz, D.C. Dunand, *Mater. Sci. Eng.* 396A (2005) 99.
- [33] T. Neeraj, M.F. Savage, J. Tatalovich, L. Kovarik, R.W. Hayes, M.J. Mills, *Philos. Mag.* 85 (2005) 279.
- [34] T.L. Anderson, *Fracture Mechanics: Fundamentals and Applications*, third ed., CRC Press, London, 2005.
- [35] R.W. Hertzberg, *Deformation and Fracture Mechanics of Engineering Materials*, fourth ed., John Wiley & Sons, Inc., New York, 1996.
- [36] R.O. Ritchie, *Int. J. Fract.* 100 (1999) 55.
- [37] Z.A. Munir, U. Anselmi-Tamburini, *Mater. Sci. Rep.* 3 (1989) 277.
- [38] A.A.M. da Silva, J.F. dos Santos, T.R. Strohaecker, *Compos. Sci. Technol.* 65 (2005) 1749.
- [39] A. Miserez, R. Müller, A. Rossoll, L. Weber, A. Mortensen, *Mater. Sci. Eng. A* 387–389 (2004) 822.
- [40] J. Segurado, C. González, J. LLorca, *Acta Mater.* 51 (2003) 2355.
- [41] T.S. Srivatsan, M. Al-Hajri, C. Smith, M. Petraroli, *Mater. Sci. Eng. A* 346 (2003) 91.
- [42] J.J. Lewandowski, C. Liu, W.H. Hunt, *Mater. Sci. Eng. A* 107 (1989) 241.
- [43] P. Poza, J. LLorca, *Mater. Sci. Eng. A* 206 (1996) 183.
- [44] S.J. Hong, H.M. Kim, D. Huh, C. Suryanarayana, B.S. Chun, *Mater. Sci. Eng. A* 347 (2003) 198.
- [45] V. Imbeni, R.K. Nalla, C. Bosi, J.H. Kinney, R.O. Ritchie, *J. Biomed. Mater. Res.* 66A (2003) 1.
- [46] Y.J. Kim, H. Chung, S.J.L. Kang, *Mater. Sci. Eng. A* 333 (2002) 343.
- [47] M. Niinomi, *Int. J. Fatigue* 29 (2007) 992.
- [48] J.J. Mason, R.O. Ritchie, *Mater. Sci. Eng. A* 231 (1997) 170.
- [49] S. Skolianos, *Mater. Sci. Eng. A* 210 (1996) 76.
- [50] Y. Sugamuri, S. Suresh, *Metall. Trans. A* 23 (1992) 2231.
- [51] J.K. Shang, W. Yu, R.O. Ritchie, *Mater. Sci. Eng. A* 102 (1988) 181.